CrystEngComm

ROYAL SOCIETY OF CHEMISTRY

PAPER

View Article Online
View Journal | View Issue

Cite this: *CrystEngComm*, 2025, **27**, 1503

Hydrochloric acid-mediated mechanical synthesis of red-emitting all-inorganic zinc halides†

Siyu Li, [a] Jiali Yao,[a] Dayang Wang, [a] Keke Huang,[a] Wensheng Yang [ab] and Renguo Xie [*a]

Received 10th December 2024,
Accepted 16th January 2025

DOI: 10.1039/d4ce01243g

rsc.li/crystengcomm

Metal halides (MHs), specifically $CsPbX_3$ (where X = Cl and Br), have garnered significant research interest due to excellent optoelectronic properties. However, most of these metal halides exhibit no red emission in the visible region. In this study, Cs_2ZnCl_4 powders in the presence of hydrochloric acid were synthesized through mechanical milling. X-ray diffraction (XRD) analyses revealed no detectable diffraction signals before or after acid treatment, suggesting a uniform crystal structure. The initial Cs_2ZnCl_4 powders displayed intrinsic blue emission centered at 486 nm, with a Photoluminescence Quantum Yield (PLQY) of approximately 5.07%. In contrast, the hydrochloric acid-treated Cs_2ZnCl_4 powder exhibited bright red emission centered at 645 nm, with a PLQY of about 12.78%. The broad emission, characterized by a full width at half maximum (FWHM) of 135 nm, was attributed to self-trapped exciton (STE) emission. X-ray photoelectron spectroscopy (XPS) analysis of Cs_2ZnCl_4 before and after acid treatment suggests that hydrochloric acid introduction may have induced distortions or defects in the coordination environment of Zn^{2+} ions. This provides a valuable route for further investigation into the optical properties of other metal halides.

Introduction

As emerging semiconductor materials, metal halides not only have excellent light absorption, tunable bandgaps and long carrier lifetimes, but also exhibit rich photovoltaic properties due to their structural diversity and tunability, which have attracted great attention in the fields of solar cells, photodetectors, light-emitting diodes (LEDs) and lasers.[1–8] Pb-based metal halide perovskites, such as $CsPbX_3$ (X = Cl, Br, and I) nanocrystals, are more advantageous in terms of luminescence performance than conventional quantum dot materials because they exhibit high fluorescence monochromaticity (FWHM less than 20 nm) and a high PLQY.[9–14] In addition, the PLQY of Pb-based perovskite materials can be significantly enhanced by optimizing the synthesis conditions, metal-ion doping or surface passivation.[15–18]

In contrast to the narrow-band emission exhibited by free excitons in lead-based perovskites, low-dimensional metal halides typically produce broadband emission resulting from self-trapped domain excitons (STEs), a characteristic attributed to their soft lattice properties. This phenomenon has generated significant interest in these luminescent materials, which offer promising applications.[19–24] Notably, lead-free zero-dimensional (0D) metal halides, with their isolated polyhedral structures, facilitate multi-exciton emission, leading to robust electron–phonon interactions and photoluminescence efficiencies of nearly 100%.[25–28] For instance, copper halides exhibiting emission within the range of 400–560 nm have been reported extensively. Silver-based halides demonstrate photoluminescence across the entire visible spectrum. Recently, fully inorganic Zn-based metal halides, such as Cs_2ZnCl_4 and Cs_3ZnCl_5 ternary halide crystals, have been synthesized and reported to exhibit excellent X-ray detectivity.[29–31] Moreover, Cr^{3+}-doped Cs_2ZnCl_4 microcrystals have achieved near-infrared (NIR) emission, opening new avenues for NIR blood vessel visualization.[32] Additionally, the blue light emission of Cs_2ZnCl_4 powder has been enhanced by doping with ions such as Cu^{2+}, Bi^{3+}, Zr^{4+}, Sb^{3+}, Mn^{2+} or Te^{4+}, which significantly increased the PLQY.[33–39] Nevertheless, few metal halides, particularly zinc-based halides, exhibit red emission.

In this study, we synthesized Cs_2ZnCl_4 powder using a solid-phase method. Subsequent treatment with hydrochloric acid transformed the originally blue-light-emitting Cs_2ZnCl_4 powder into one that exhibits bright red emission with a peak of 645 nm. The X-ray diffraction (XRD) measurement

[a] *State Key Laboratory of Inorganic Synthesis and Preparative Chemistry, College of Chemistry Jilin University, Changchun 130012, China.*
E-mail: renguoxie@jlu.edu.cn
[b] *Engineering Center for Nanomaterials, Henan University, Kaifeng, 475004, China*
† Electronic supplementary information (ESI) available. See DOI: https://doi.org/10.1039/d4ce01243g

shows the same diffraction characterization, and no detectable change was observed before and after acid treatment. This red emissive characterization might be attributed to the introduction of hydrochloric acid, as determined by X-ray photoelectron spectroscopy (XPS), where hydrochloride was detected in the sample treated with acid. Accordingly, the broad emission should have originated from STEs as confirmed by the result from variable temperature spectroscopy measurements. This red emissive characterization in zinc-based halides would promote their further applications in the optoelectronic field.

Experimental

Materials

$ZnCl_2$ (98.0%) was purchased from Alfa Aesar. CsCl (99.9%) was purchased from Aladdin Industrial Corporation. All powder materials were stored in a nitrogen-filled glovebox. HCl (36–38 wt% in H_2O) was purchased from Beijing Chemical Reagent Ltd. All the chemicals and materials were used without any further purification.

Synthesis of Cs_2ZnCl_4 MHs

To produce Cs_2ZnCl_4, typically, CsCl (1 mmol) and $ZnCl_2$ (0.5 mmol) were put together into a 25 mL zirconia jar with about 25–35 zirconia balls, and all operations were carried out under nitrogen protection in a glovebox. Subsequently, the jar was closed and transferred to a ball-milling grinder (QM-3SP04). Ball milling was carried out at a frequency of 35 Hz for 4 h to produce Cs_2ZnCl_4 as a white powder with weak blue luminescence under 254 nm UV irradiation.

Acid treatment of Cs_2ZnCl_4 MHs

After adequate grinding of all MHs, 200 μL of HCl was added to Cs_2ZnCl_4. Subsequently, the grinding was continued for 30 min.

pH measurements

All samples were dried in a vacuum drying oven at 100° for 2 h. Then, 0.2 mmol of as-prepared and acid-treated Cs_2ZnCl_4 were added to 2 mL of H_2O, respectively. All samples were sonicated for 5 min until they were fully dissolved in water, followed by centrifugation at 1000 rpm for 20 minutes, and the supernatant was tested for pH.

Characterization method

X-ray photoelectron spectroscopy (XPS) was conducted with a Thermo ESCALAB 250 Xi instrument. Powder wide-angle X-ray diffraction (XRD) patterns were measured with a Philips PW1830 X-ray diffractometer with Cu Kα radiation (λ = 1.54056 Å) in a 2q (q: diffraction angle) range from 10° to 70°. UV-visible absorption spectra were obtained with a U4100 UV-visible spectrophotometer (Shimadzu). Photoluminescence (PL) spectra and time-resolved and temperature-dependent PL spectra were acquired on a steady-state fluorescence spectrometer (Edinburgh FLS920). Mean fluorescence lifetimes $\langle t \rangle$ for multi-exponential iterative fitting were calculated from the decay time and the pre-exponential factors. Fluorescence quantum yields were estimated using an FLS920 fluorescence spectrometer with a xenon lamp and Quanta-φ integrating sphere.

Results and discussion

In our previous work, a green and efficient solid-state synthesis method was used for the synthesis of various metal halides. Here, we directly synthesized pure-phase Cs_2ZnCl_4 powder through directly milling a CsCl and $ZnCl_2$ mixture at a frequency of 35 Hz for 4 h. Subsequently, 200 μL of hydrochloric acid (HCl) was rapidly added to an agate jar containing the pure-phase Cs_2ZnCl_4, and milling was continued for 30 minutes. The resulting pure-phase Cs_2ZnCl_4 powder exhibited blue light emission under a 254 nm UV lamp, indicating the intrinsic luminescence of Cs_2ZnCl_4. In contrast, the as-prepared powder further ground for 30 min in the presence of chloride acid demonstrated bright red emission under the 254 nm UV lamp, as illustrated in Fig. 1a. Fig. 1b demonstrates X-ray diffraction (XRD) patterns of the samples before and after acid treatment. The crystal structures of the resulting zinc halides align with standard powder diffraction files (PDFs). The corresponding generic crystal structures viewed down the a-axis are provided in Fig. S1† where Cs_2ZnCl_4 crystallizes in an orthorhombic structure with the space group *Pnma*, where the disconnected $[ZnCl_4]^{2-}$ tetrahedra are separated by Cs^+ cations, forming a soft lattice that facilitates local structural deformation under thermal stimulation, thus enabling optical modulation.[40,41] By comparison, no detectable diffraction signals were observable for the sample with acid treatment, suggesting that the samples before and after the introduction of the acid have a uniform crystal structure. Nevertheless, the diffraction peaks of the acid-treated samples shifted slightly toward smaller angles, suggesting that parameters such as the Zn–Cl bond length and the Cl–Zn–Cl bond angle of the acid-treated $[ZnCl_4]^{2-}$ tetrahedra should be altered, subsequently affecting the degree of distortion of the tetrahedra. Fig. 1c and d exhibit the absorption and steady-state photoluminescence (PL) spectra of Cs_2ZnCl_4 powders before and after the introduction of hydrochloric acid. The UV-vis absorption spectra of both samples almost have the same optical profile in which a weak absorption peak at approximately 390 nm was observed, although the sample treated with the acid exhibits stronger absorption properties. The untreated sample exhibits a weak PL peak centered at 486 nm with a FWHM of 82 nm under an excitation wavelength of 270 nm. This optical property is similar to that reported previously in our work. In contrast, the Cs_2ZnCl_4 sample treated with hydrochloric acid displays a significant emission peak

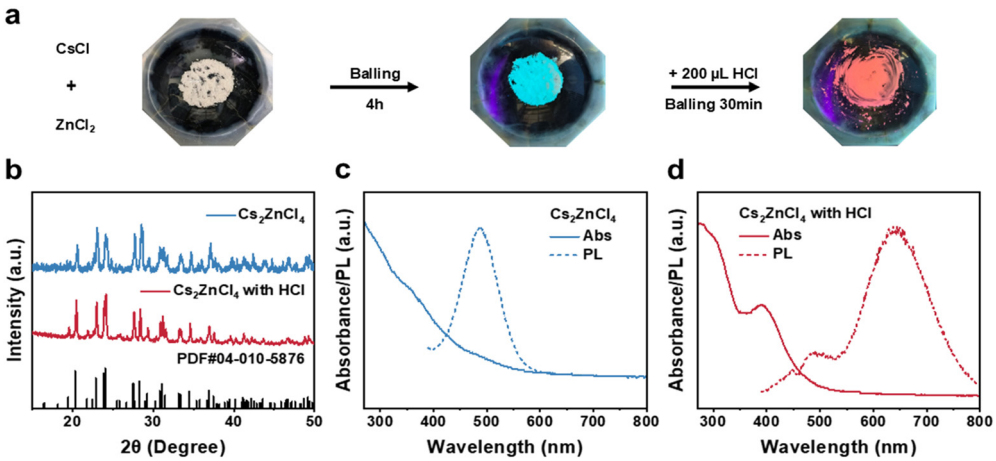

Fig. 1 (a) Photographs depicting the schematic diagram of the synthetic process, as well as the changes in color (under ambient light) and luminescence (under a UV lamp), illustrating the mechanochemical synthesis of Cs_2ZnCl_4 achieved through the grinding of CsCl and $ZnCl_2$. (b) XRD patterns of Cs_2ZnCl_4 powders before and after hydrochloric acid treatment. Absorption and emission spectra of (c) Cs_2ZnCl_4 powders and (d) hydrochloric acid-treated Cs_2ZnCl_4.

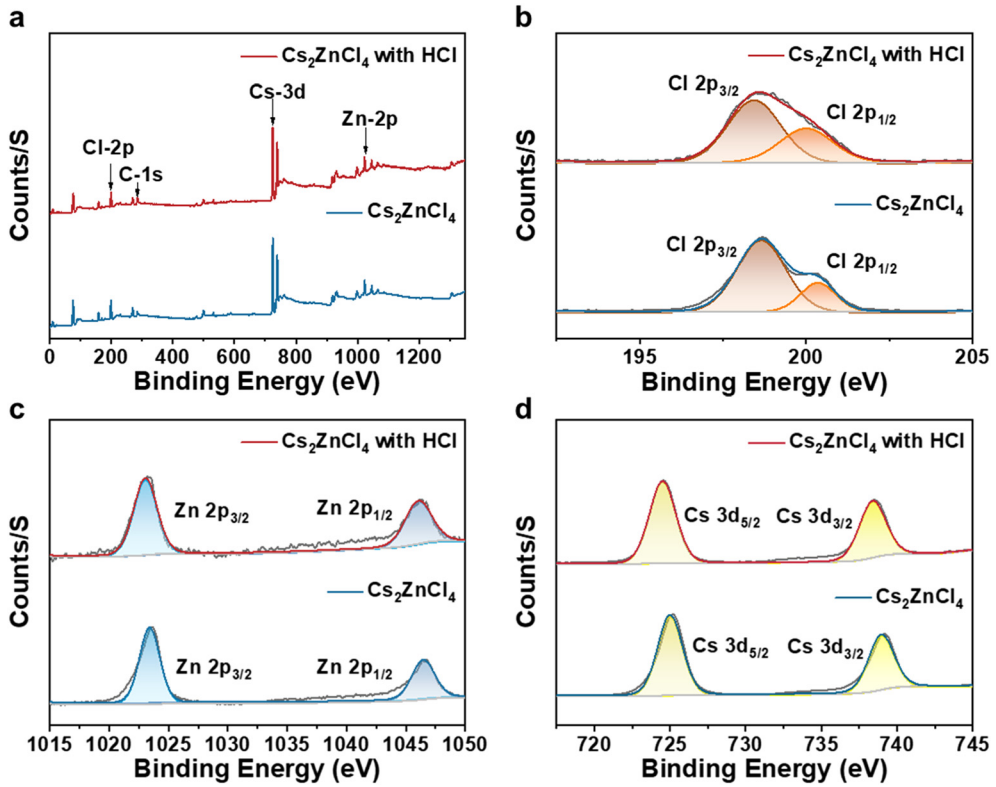

Fig. 2 (a) XPS full spectrum analysis and XPS split-fit spectra of (b) Cl 2p, (c) Zn 2p and (d) Cs 3d of Cs_2ZnCl_4 before and after hydrochloric acid treatment.

centered at 645 nm with an FWHM of 135 nm and a large Stokes shift under the same excitation wavelength. To the best of our knowledge, this is the first report on red-emissive all-inorganic zinc halides.

To further investigate the origin of the red emission from hydrochloric acid-treated Cs_2ZnCl_4, we conducted X-ray photoelectron spectroscopy (XPS) analysis on the samples both before and after acid treatment. Fig. 2a presents the XPS full-scan spectra of untreated and hydrochloric acid-treated Cs_2ZnCl_4. The observed peak positions align with the expected chemical states of the elements (Cs^+, Zn^{2+}, and Cl^-). Subsequently, split peaks were fitted to the fine XPS spectra of Cl 2p, Zn 2p, and Cs 3d. The bimodal peaks for Cl $2p_{3/2}$ and Cl $2p_{1/2}$ in untreated Cs_2ZnCl_4 were identified at 198.54 eV and 200.15 eV, respectively, whereas those in the hydrochloric acid-treated sample were found at 198.43 eV

Table 1 pH and quantities of H^+ in a given Cs_2ZnCl_4 sample before and after the acid treatment

Material	pH	$n(H^+)$/mmol
Cs_2ZnCl_4	3.13	1.48×10^{-3}
Cs_2ZnCl_4 with HCl	1.21	6.16×10^{-2}

and 200.03 eV (Fig. 2b). Additionally, the peaks for Zn $2p_{3/2}$ and Zn $2p_{1/2}$ were located at 1023.42 eV and 1046.31 eV in untreated Cs_2ZnCl_4, compared to 1023.13 eV and 1046.02 eV in the hydrochloric acid-treated sample (Fig. 2c), while the peaks for Cs $3d_{3/2}$ and Cs $3d_{5/2}$ show minor shifts from 724.6 eV and 738.5 eV to 725.4.42 eV and 738.91 eV (Fig. 2d), respectively, with and without the presence of acid. The positions of these peaks shifted slightly toward a lower binding energy, indicating that hydrochloric acid treatment may have modified the coordination environment of the Zn^{2+} ion or distorted the $[ZnCl_4]^{2-}$ tetrahedron. This observation corresponds to the shift in the XRD peaks of Cs_2ZnCl_4, both with and without acid treatment. By integrating the areas of the corresponding signal peaks for various elements, we compared the Cl/Zn molar ratios in Cs_2ZnCl_4 before and after hydrochloric acid treatment, yielding values of 4.15 and 4.48, respectively. This change suggests that additional Cl^- was introduced into the samples during the hydrochloric acid treatment, resulting in a slight increase in the Cl/Zn molar ratio. The deviation of the Cl/Zn molar ratio in untreated Cs_2ZnCl_4 from the theoretical value of 4 may arise from variations in the electron detection efficiency among different elements in the XPS analyses.

In addition to determining Cl^- ions in the samples, we also conducted H^+ ion measurements for samples with and without hydrochloric acid-treated Cs_2ZnCl_4. To remove the excess HCl completely from the samples, two specimens were dried in a vacuum drying oven at 100 °C for 2 hours. The resulting powders (0.2 mmol each) were subsequently placed in individual 2 mL volumes of deionized water, treated with ultrasound for 20 minutes, and the pH of the supernatant was then measured using a calibrated electrode. Following the acid treatment, the pH decreased from 3.13 to 1.21, and the concentration of H^+ increased from 1.48×10^{-3} mmol to 6.16×10^{-2} mmol (Table 1). This study confirms the presence of H^+ ions in Cs_2ZnCl_4. For comparison, we also estimated the excess Cl^- in Cs_2ZnCl_4 (0.2 mmol) before and after the acid treatment to be approximately 0.066 mmol based on the atomic ratio of Cl/Zn determined by X-ray photoelectron spectroscopy (XPS). The amount of excess H^+ determined from the pH test was approximately 0.060 mmol, which is nearly 1 : 1. This finding suggests that acid-treated Cs_2ZnCl_4 should contain hydrochloric acid, which could be integral to the observed red emission.

We characterized the PLQY of the Cs_2ZnCl_4 powder before and after the treatment with hydrochloric acid, as illustrated in Fig. 3a. The sample without the acid exhibits a PLQY of 5.07%, while the hydrochloric acid-treated Cs_2ZnCl_4 powder demonstrated a significant increase in red light emission, achieving a PLQY of 12.78%. Furthermore, additional efforts were undertaken to vary the concentration of hydrochloric acid. However, the results indicated that the PLQY of Cs_2ZnCl_4 powders treated with different hydrochloric acid concentrations remained approximately constant. The decay curves of the hydrochloric acid-treated Cs_2ZnCl_4 were accurately fitted using a biexponential function, as shown in Fig. 3b and detailed in Table S1.† The average lifetime of the hydrochloric acid-treated Cs_2ZnCl_4 was found to be approximately 8.42 μs.

The intrinsic emission mechanism of the HCl-treated Cs_2ZnCl_4 was further characterized by the emission wavelength-dependent PLE spectra and excitation wavelength-dependent and temperature-dependent PL spectra. As shown in Fig. 4a and b, when the monitoring emission was changed from 630 nm to 670 nm, the PLE spectra remained unchanged at various excitation wavelengths. Similarly, when the excitation was varied from 250 nm to 270 nm, the PL spectra exhibited the same features as well. Such identical features of the PLE and PL spectra at different wavelengths indicate that the red

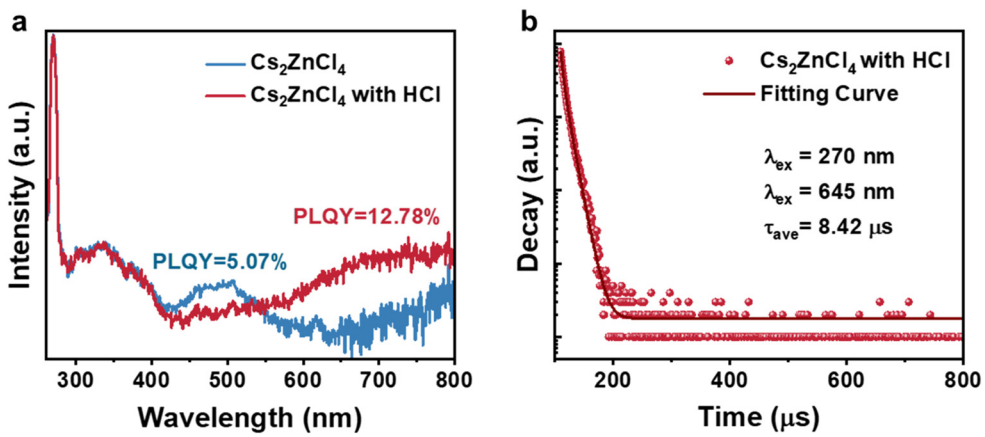

Fig. 3 (a) PLQY spectra of the Cs_2ZnCl_4 powder before and after hydrochloric acid treatment. (b) Fitted spectra of the PL decay lifetime of hydrochloric acid-treated Cs_2ZnCl_4 measured at 270 nm laser irradiation.

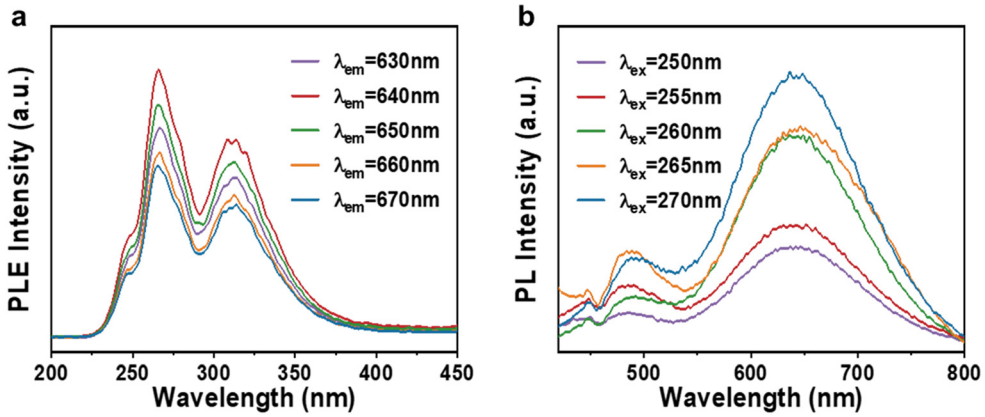

Fig. 4 (a) PLE spectra and the (b) PL spectra of hydrochloric acid-treated Cs_2ZnCl_4 measured under different excitations and different emissions, respectively.

emission originates from the recombination of the same excited state instead of the defect emission.[42] Temperature-dependent PL spectra were measured for HCl-treated Cs_2ZnCl_4 in the range of 138 K to 318 K (Fig. 5a). The intensity of the emission peaks gradually decreases as the temperature gradually increases from 138 K to 318 K, while the FWHM broadens. This result indicates that more photons couple with excitons at higher temperatures, thus accelerating the nonradiative irradiation process. In addition, a slight blue shift of the PL peak position occurs with increasing temperature, which is due to the weakening of the crystal field strength and the narrowing of the splitting energy of the excited state as a result of thermal expansion.[43,44] Fig. 5b shows the integral PL intensity (I) of acid-treated Cs_2ZnCl_4 as a function of the reciprocal of temperature ($1/T$). The exciton binding energy (E_b) can be derived from the following equation:[45]

$$I(T) = \frac{I_0}{\left[1 + A_{\exp}\left(\frac{E_b}{k_B T}\right)\right]}$$

where $I(T)$ is the intensity at temperature T, I_0 is the

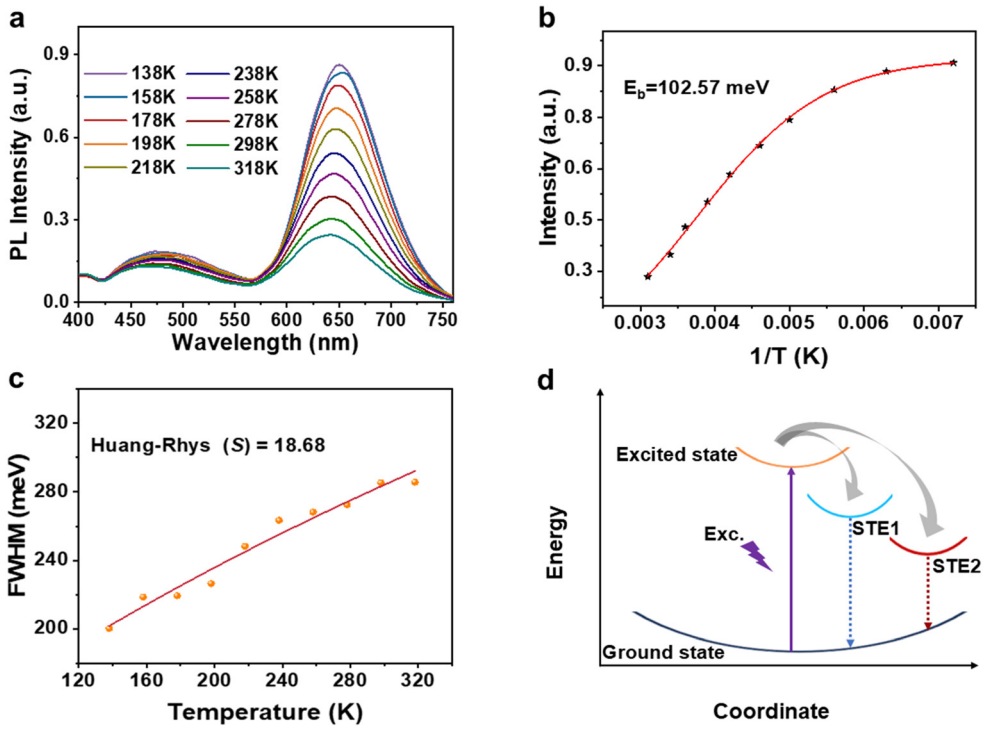

Fig. 5 (a) Temperature-dependent PL spectra of acid-treated Cs_2ZnCl_4 from 138 K to 318 K (λ_{ex} = 270 nm). (b) Fitting results of the integrated PL emission intensity as a function of the reciprocal of temperature. (c) Fitting results of the FWHM as a function of temperature. (d) The coordinate diagram of the photophysical processes in hydrochloric acid-treated Cs_2ZnCl_4.

emission intensity of 0 K, A is the proportional coefficient, and k_B is the Boltzmann constant. By fitting the curve as shown in Fig. 5b, it turns out that the exciton binding energy (E_b) for HCl-treated Cs_2ZnCl_4 is calculated to be 102.57 meV, which is much larger than that of conventional 3D perovskites or the thermal energy at room temperature (~25 meV).[46] Such a high E_b is attributed to its 0D electronic dimensionality. In this 0D structure, photogenerated excitons are strongly confined in individual $[ZnCl_4]^{2-}$ octahedra, resulting in a high E_b with a stable bright emission. Fig. 5c shows the temperature-dependent FWHM curve of HCl-treated Cs_2ZnCl_4. The Huang–Rhys factor (S) and the phonon frequency ($\hbar\omega_{phonon}$) can be derived by the following equation:[47]

$$\mathrm{FWHM}(T) = 2.36\sqrt{S}\hbar\omega_{\mathrm{phonon}}\sqrt{\coth\frac{\hbar\omega_{\mathrm{phonon}}}{2k_BT}}$$

By fitting the temperature-dependent full width at half maximum (FWHM) curve, the S factor was determined to be 18.68. The relatively high Huang–Rhys factor and phonon energy indicate strong electron–phonon coupling in acid-treated Cs_2ZnCl_4. Combined with a large Stokes shift and significant Huang–Rhys factor, as well as phonon frequency, the emission mechanism of HCl-treated Cs_2ZnCl_4 is likely attributed to the formation of self-trapped excitons (STEs).[48] The exciton self-trapping process of HCl-treated Cs_2ZnCl_4 is schematically illustrated in Fig. 5d. Upon photoexcitation, the electrons are promoted from the ground state to a high-energy free-exciton excited state. This transition induces the formation of a self-trapped excited state, which is attributed to lattice deformation driven by strong electron–phonon coupling. Subsequently, the excited electrons undergo rapid relaxation and intersystem crossing, transitioning from the free-exciton to self-trapped excited states. Finally, broadband red emission with a large Stokes shift is observed.

Self-trapped excitons are consistently observed in metal halide crystals. Previous studies have indicated that Cs_2ZnCl_4 powder exhibits only a weak blue emission, suggesting the presence of a single self-trapped state for intrinsic STEs (Fig. S2†). Furthermore, the PL emission of intrinsic STEs decreases with increasing temperature. This reduction may be attributed to several factors, including the abundance of structural defects within the Cs_2ZnCl_4 powder, thermal dissociation of excitons, and enhanced electron–phonon coupling associated with intrinsic STEs, which collectively contribute to non-radiative decay and diminished emission.[33] Following hydrochloric acid treatment, additional extrinsic STE states are observed. The radiative transitions from the intrinsic STE and extrinsic STE to the ground state correspond to PL bands at wavelengths of 486 nm and 645 nm, respectively. The emergence of extrinsic STE states may be attributed to the distortion of the coordination environment of Zn^{2+} ions or the introduction of defects resulting from hydrochloric acid treatment.[49] Acid-treated Cs_2ZnCl_4 also demonstrates good environmental stability, as evidenced by its sustained bright red emission under a 254 nm UV lamp after 15 days of exposure (Fig. S3†).

Conclusions

In summary, "red-emissive" zinc-based halide powders were synthesized through a mechanical milling strategy in the presence of hydrochloric acid. XRD analyses revealed no detectable diffraction signals in the samples before or after acid treatment, indicating that the synthesized samples maintained a consistent crystal structure. The acid-treated Cs_2ZnCl_4 exhibited bright red emission centered at 645 nm, with a PLQY of approximately 12.78%. XPS analysis confirmed the Cl and H ions in the hydrochloric acid-treated Cs_2ZnCl_4 samples. Therefore, the nature of the red emission can be attributed to the presence of HCl in the sample. Experimental studies reveal that the intrinsic photoluminescence nature of the sample originates from STEs. The red-emissive properties of zinc-based halides not only enhance their potential applications in the optoelectronic field but also provide a valuable pathway for further investigations into the optical properties of other metal halides.

Data availability

The data supporting this article are available from the corresponding author, Renguo Xie, upon reasonable request.

Author contributions

Siyu Li carried out the experiments and wrote the manuscript. Jiali Yao aided with testing and characterization. Jiali Yao, Dayang Wang, Keke Huang, and Wensheng Yang helped with the analysis of the experimental data. Renguo Xie designed the organization of the manuscript and revised it. All authors contributed to the general discussion.

Conflicts of interest

There are no conflicts to declare.

Acknowledgements

This work is financially supported by the National Natural Science Foundation of China (Grant No. 51872114, 21932003, 22371090 and 22161132009).

References

1 H. P. Zhou, Q. Chen, G. Li, S. Luo, T. B. Song, H. S. Duan, Z. R. Hong, J. B. You, Y. S. Liu and Y. Yang, *Science*, 2014, **345**, 542–546.
2 N. J. Jeon, J. H. Noh, Y. C. Kim, W. S. Yang, S. Ryu and S. I. Seok, *Nat. Mater.*, 2014, **13**, 897–903.
3 L. T. Dou, Y. Yang, J. B. You, Z. R. Hong, W. H. Chang, G. Li and Y. Yang, *Nat. Commun.*, 2014, **5**, 6.

4 P. Ramasamy, D. H. Lim, B. Kim, S. H. Lee, M. S. Lee and J. S. Lee, *Chem. Commun.*, 2016, **52**, 2067–2070.
5 J. Byun, H. Cho, C. Wolf, M. Jang, A. Sadhanala, R. H. Friend, H. Yang and T. W. Lee, *Adv. Mater.*, 2016, **28**, 7515–7520.
6 Z. G. Xiao, R. A. Kerner, L. F. Zhao, N. L. Tran, K. M. Lee, T. W. Koh, G. D. Scholes and B. P. Rand, *Nat. Photonics*, 2017, **11**, 108–115.
7 Q. Zhang, R. Su, W. N. Du, X. F. Liu, L. Y. Zhao, S. T. Ha and Q. H. Xiong, *Small Methods*, 2017, **1**, 12.
8 Q. Zhang, R. Su, X. F. Liu, J. Xing, T. C. Sum and Q. H. Xiong, *Adv. Funct. Mater.*, 2016, **26**, 6238–6245.
9 X. Lu, Y. Hu, J. Z. Guo, C. F. Wang and S. Chen, *Adv. Sci.*, 2019, **6**, 9.
10 Y. W. Pan, Y. F. Zhang, W. M. Kang, N. P. Deng, Z. R. Yan, W. Sun, X. Y. Kang and J. Ni, *Mater. Adv*, 2022, **3**, 4053–4068.
11 J. De Roo, M. Ibáñez, P. Geiregat, G. Nedelcu, W. Walravens, J. Maes, J. C. Martins, I. Van Driessche, M. V. Koyalenko and Z. Hens, *ACS Nano*, 2016, **10**, 2071–2081.
12 Y. B. Zhao, C. Xie, X. Zhang and P. Yang, *ACS Appl. Nano Mater.*, 2021, **4**, 5478–5485.
13 L. Protesescu, S. Yakunin, M. I. Bodnarchuk, F. Krieg, R. Caputo, C. H. Hendon, R. X. Yang, A. Walsh and M. V. Kovalenko, *Nano Lett.*, 2015, **15**, 3692–3696.
14 S. N. Guo, H. Wu, D. Wang and J. X. Wang, *Langmuir*, 2021, **37**, 11520–11525.
15 J. D. Lin, Y. X. Lu, X. Y. Li, F. Huang, C. B. Yang, M. L. Liu, N. Z. Jiang and D. Q. Chen, *ACS Energy Lett.*, 2021, **6**, 519–528.
16 F. Di Stasio, S. Christodoulou, N. J. Huo and G. Konstantatos, *Chem. Mater.*, 2017, **29**, 7663–7667.
17 V. G. V. Dutt, S. Akhil and N. Mishra, *Nanoscale*, 2021, **13**, 14442–14449.
18 F. Liu, Y. H. Zhang, C. Ding, S. Kobayashi, T. Izuishi, N. Nakazawa, T. Toyoda, T. Ohta, S. Hayase, T. Minemoto, K. Yoshino, S. Y. Dai and Q. Shen, *ACS Nano*, 2017, **11**, 10373–10383.
19 Y. Y. Wu, W. B. Fan, Z. R. Gao, Z. Tang, L. Lei, X. F. Sun, Y. L. Li, H. L. Cai and X. S. Wu, *Nano Energy*, 2020, **77**, 11.
20 T. M. Jiang, W. B. Ma, H. Zhang, Y. Tian, G. Lin, W. G. Xiao, X. Yu, J. B. Qiu, X. H. Xu, Y. Yang and D. X. Ju, *Adv. Funct. Mater.*, 2021, **31**, 9.
21 T. Hu, M. D. Smith, E. R. Dohner, M. J. Sher, X. X. Wu, M. T. Trinh, A. Fisher, J. Corbett, X. Y. Zhu, H. I. Karunadasa and A. M. Lindenberg, *J. Phys. Chem. Lett.*, 2016, **7**, 2258–2263.
22 M. D. Smith and H. I. Karunadasa, *Acc. Chem. Res.*, 2018, **51**, 619–627.
23 Z. Yuan, C. K. Zhou, Y. Tian, Y. Shu, J. Messier, J. C. Wang, L. J. van de Burgt, K. Kountouriotis, Y. Xin, E. Holt, K. Schanze, R. Clark, T. Siegrist and B. W. Ma, *Nat. Commun.*, 2017, **8**, 7.
24 L. L. Mao, P. J. Guo, M. Kepenekian, I. Hadar, C. Katan, J. Even, R. D. Schaller, C. C. Stoumpos and M. G. Kanatzidis, *J. Am. Chem. Soc.*, 2018, **140**, 13078–13088.
25 B. Park, H. Yang, T. H. Ha, H. S. Park, S. J. Oh, Y. S. Ryu, Y. Cho, H. S. Kim, J. Oh, D. K. Lee, C. Kim, T. Lee, M. Seo, J. Choi, Y. M. Jhon, D. H. Woo, S. Lee, S. H. Kim, H. J. Lee, S. C. Jun, H. S. Song, T. H. Park and J. H. Kim, *Adv. Mater.*, 2018, **30**, 8.
26 L. Zhou, J. F. Liao, Z. G. Huang, J. H. Wei, X. D. Wang, W. G. Li, H. Y. Chen, D. B. Kuang and C. Y. Su, *Angew. Chem., Int. Ed.*, 2019, **58**, 5277–5281.
27 B. M. Benin, D. N. Dirin, V. Morad, M. Wörle, S. Yakunin, G. Rainò, O. Nazarenko, M. Fischer, I. Infante and M. V. Kovalenko, *Angew. Chem., Int. Ed.*, 2018, **57**, 11329–11333.
28 M. Chen, M. G. Ju, A. D. Carl, Y. X. Zong, R. L. Grimm, J. J. Gu, X. C. Zeng, Y. Y. Zhou and N. P. Padture, *Joule*, 2018, **2**, 558–570.
29 K. Takahashi, M. Arai, M. Koshimizu, Y. Fujimoto, T. Yanagida and K. Asai, *Jpn. J. Appl. Phys.*, 2020, **59**, 5.
30 N. Yahaba, M. Koshimizu, Y. Sun, T. Yanagida, Y. Fujimoto, R. Haruki, F. Nishikido, S. Kishimoto and K. Asai, *Appl. Phys. Express*, 2014, **7**, 4.
31 K. Sugawara, M. Koshimizu, T. Yanagida, Y. Fujimoto, R. Haruki, F. Nishikido, S. Kishimoto and K. Asai, *Opt. Mater.*, 2015, **41**, 53–57.
32 T. C. Zheng, H. X. Yang, H. L. Lu, Y. L. Liu, Y. Li, C. X. Peng, L. B. Zhang and X. Y. Li, *J. Lumin.*, 2024, **271**, 8.
33 X. M. Dong and R. K. Pan, *Phys. B*, 2024, **676**, 5.
34 D. X. Zhu, M. L. Zaffalon, V. Pinchetti, R. Brescia, F. Moro, M. Fasoli, M. Fanciulli, A. Tang, I. Infante, L. De Trizio, S. Brovelli and L. Manna, *Chem. Mater.*, 2020, **32**, 5897–5903.
35 X. Y. Zhao, X. S. Zhang, X. K. Gong, X. R. Yuan, M. X. Chen, S. W. Huang, B. Z. Zhou, J. P. Xu and L. Li, *Inorg. Chem. Front.*, 2023, **11**, 71–84.
36 Y. Tian, Q. Wei, L. Duan and C. Peng, *Molecules*, 2024, **29**, 1651.
37 Y. Guo, J. K. Chen, B. Chen, W. L. Zheng, X. Zhang, H. Suo, F. J. Chun, X. H. Wei and F. Wang, *Mater. Today Phys.*, 2023, **35**, 101111.
38 T. C. Zheng, H. X. Yang, Y. L. Liu, Y. Li, Q. Huang, L. B. Zhang and X. Y. Li, *Inorg. Chem.*, 2023, **62**, 17352–17361.
39 X. X. Liu, C. D. Peng, L. J. Zhang, D. Y. Guo and Y. X. Pan, *J. Mater. Chem. C*, 2022, **10**, 204–209.
40 X. X. Liu, C. D. Peng, L. J. Zhang, D. Y. Guo and Y. X. Pan, *J. Mater. Chem. C*, 2021, **10**, 204–209.
41 I. Romdhane, A. Ajmi, M. Ben Bechir, R. Barille and A. Ben Rhaiem, *RSC Adv.*, 2024, **14**, 36253–36263.
42 W. R. Gao, G. D. Niu, L. X. Yin, B. Yang, J. H. Yuan, D. D. Zhang, K. H. Xue, X. S. Miao, Q. S. Hu, X. Y. Du and J. Tang, *ACS Appl. Electron. Mater.*, 2020, **2**, 2242–2249.
43 Z. N. Zhang, H. M. Cheng, S. Y. Teng, K. K. Huang, D. Y. Wang, W. S. Yang and R. G. Xie, *Inorg. Chem.*, 2022, **61**, 20552–20560.
44 L. Y. Lian, P. Zhang, J. B. Gao, D. L. Zhang and J. B. Zhang, *Chem. Mater.*, 2023, **35**, 9339–9345.
45 M. Baranowski and P. Plochocka, *Adv. Energy Mater.*, 2020, **10**, 15.

46 S. M. Lee, C. J. Moon, H. Lim, Y. Lee, M. Y. Choi and J. Bang, *J. Phys. Chem. C*, 2017, **121**, 26054–26062.
47 M. Y. Jin, W. Zheng, Z. L. Gong, P. Huang, R. F. Li, J. Xu, X. W. Cheng, W. Zhang and X. Y. Chen, *Nano Res.*, 2022, **15**, 6422–6429.
48 F. Jiang, Z. N. Wu, M. Lu, Y. B. Gao, X. Li, X. Bai, Y. Ji and Y. Zhang, *Adv. Mater.*, 2023, **35**, 13.
49 M. Watanabe, H. Takahashi, K. Uematsu, M. Sato, T. Masaki, D. H. Yoon and K. Toda, *J. Ceram. Soc. Jpn.*, 2022, **130**, 458–463.